

# Interactive segmentation via deep learning and B-spline explicit active surfaces

Helena Williams<sup>1,3,4</sup>, João Pedrosa<sup>2</sup>, Laura Cattani<sup>1</sup>, Susanne Housmans<sup>1</sup>, Tom Vercauteren<sup>3</sup>, Jan Deprest<sup>1</sup>, and Jan D'hooge<sup>4</sup>

<sup>1</sup> Department of Obstetrics and Gynaecology, University Hospitals Leuven, Belgium

<sup>2</sup> INESC TEC - Institute for Systems and Computer Engineering, Technology and Science, Porto Portugal

<sup>3</sup> School of Biomedical Engineering & Imaging Sciences, King's College London, UK

<sup>4</sup> Department of Cardiovascular Sciences, KU Leuven, Belgium

**Abstract.** Automatic medical image segmentation via convolutional neural networks (CNNs) has shown promising results. However, they may not always be robust enough for clinical use. Sub-optimal segmentation would require clinician's to manually delineate the target object, causing frustration. To address this problem, a novel interactive CNN-based segmentation framework is proposed in this work. The aim is to represent the CNN segmentation contour as B-splines by utilising B-spline explicit active surfaces (BEAS). The interactive element of the framework allows the user to precisely edit the contour in real-time, and by utilising BEAS it ensures the final contour is smooth and anatomically plausible. This framework was applied to the task of 2D segmentation of the levator hiatus from 2D ultrasound (US) images, and compared to the current clinical tools used in pelvic floor disorder clinic (4DView, GE Healthcare; Zipf, Austria). Experimental results show that: 1) the proposed framework is more robust than current state-of-the-art CNNs; 2) the perceived workload calculated via the NASA-TLX index was reduced more than half for the proposed approach in comparison to current clinical tools; and 3) the proposed tool requires at least 13 seconds less user time than the clinical tools, which was *significant* ( $p=0.001$ ).

## 1 Introduction

Medical image segmentation of anatomical structures can be used for disease diagnosis [6]. Manual segmentation requires expertise, time and is prone to error, therefore, automatic methods are desirable. Deep learning-based solutions with convolutional neural networks (CNNs) have been extensively explored [24,19]. However, their impressive average performance has not yet led to wide clinical adoption [4]. Medical images pose serious challenges to automatic methods, as they can be sensitive to small differences between training and testing data, due to such factors as image quality, imaging protocols (i.e. imaging acquisition discrepancies), pathology, and patient variation [7,13,27,23]. Therefore, it is important for clinical impact and acceptance, to be able to recover from a poor result

and address the limitations of automatic segmentation. As the clinician remains liable for the measurements obtained for diagnosis, if the automatic method is incorrect, it is the responsibility of the clinician to identify the problem and correct the segmentation. Interactive segmentation with an intuitive mechanism, for smart correction of poor segmentation, may solve these problems, and give liability to the clinician without them having to manually re-segment, which is not time efficient and may cause frustration. This work is motivated to combine state-of-the-art CNN segmentation with an user interaction tool, which allows the clinician to view, correct (if needed) and save the desired segmentation.

An extensive range of CNN-based interactive methods have been proposed [21], exploiting bounding boxes [20], scribbles [16,26], extreme points [17] or clicks [12]. These achieved higher accuracy and robustness than their automatic counterparts, however, they can require a high cognitive load and understanding. In addition, the user still relies on the CNN to segment correctly and is not always able to edit the contour precisely, in an adequate and time efficient manner.

In this paper, an interactive segmentation tool for 2D semantic medical image segmentation is proposed. The tool is composed of three stages. In the first stage, a CNN automatically obtains an initial segmentation, this feeds as an initialisation to an active contour segmentation framework called B-spline explicit active surfaces (BEAS) [2], which smooths the contour to be more biologically plausible (acting as a post-processing step), and thirdly a novel algorithm which allows the user to interact with the contour in real-time was implemented.

The proposed approach is compared with manual tools used in clinic for 2D segmentation of the levator hiatus in pelvic floor disorder assessment: “Point” and “Trace” both available on the ultrasound (US) software 4DView (GE Healthcare; Zipf, Austria), and compared with a state-of-the-art scribble-based approach referred to as UGIR [26]. The segmentation methods are evaluated on 30 2D US images, the time taken to segment to a clinically acceptable level, and the perceived workload are measured and compared. The contributions of this work are four-fold: 1) A novel CNN-based interactive framework for 2D segmentation is proposed; 2) the interactive element works in real time and requires less user time and perceived workload than clinical methods and UGIR; 3) the method utilises the BEAS framework to ensure the final contour is more biologically plausible than the CNN segmentation, acting as a novel post-processing method; and 4) a new energy term is introduced that is dependent on the probability map of the CNN output, which has not been utilised in BEAS before.

## 2 Material and Methods

### 2.1 Proposed pipeline

The proposed pipeline is composed of three sequential parts: a 2D CNN which segments the target object (levator hiatus) from the US image; a BEAS-based post-processing method which smooths the CNN segmentation and represents the segmentation boundary as a B-spline explicit active surface; and a novel

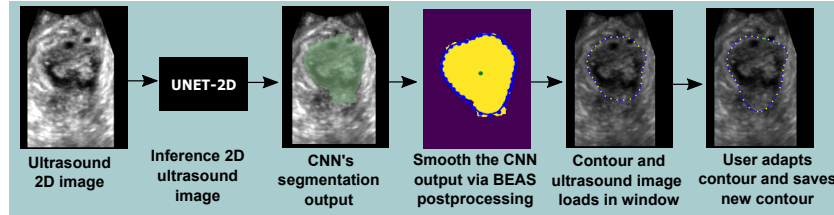


**Fig. 1.** The proposed pipeline that accepts a 2D US, segments the target object via CNN segmentation, smooths the segmentation and loads it in a window, to allow the user to adapt the contour via BEAS interaction.

algorithm (implemented in a graphical user interface (GUI) referred to as Beyond), that allows the user to adapt the contour in real-time while benefiting from BEAS’s active model properties. The framework is shown in Fig. 1. The first task of the pipeline, automatically defined the levator hiatus from the US image. This elaborates from previous work where 2D U-Net was used [6,15]. The segmentation is fed as input to the following task.

**BEAS-based smoothing** The second task utilises the BEAS framework [2]. A 2D version of BEAS is applied to the CNN segmentation after thresholding, to represent the CNN segmentation boundary as B-splines. The concept of BEAS, is to regard the boundary of a target object (i.e. the CNN segmentation) as an explicit function, where one of the coordinates of the boundary, is given explicitly as a function of the remaining coordinates. As the contour is a closed 2D object, the boundary can be represented in the polar domain, and the contour radius is represented as an explicit function of the polar angle, *i.e.*  $\rho = \psi(\theta)$ . Inspired by Bernard et al. [5], the explicit function  $\psi$  can be expressed as a linear combination of B-spline basis functions [25,5,2],

$$\rho = \sum_{\mathbf{k} \in \mathbb{Z}^{n-1}} c[\mathbf{k}] \beta^d \left( \frac{\theta}{h} - \mathbf{k} \right). \quad (1)$$

$\beta^d(\cdot)$  is the uniform symmetric  $n-1$ -dimensional B-spline of degree  $d$ .  $\psi(\theta)$  is separable and built as the product of  $n-1$  1D B-splines. The knots of the B-splines are located on a regular grid defined on the polar coordinate system, with regular spacing given by  $h$ . The B-spline coefficients are gathered in  $c[\mathbf{k}]$ .

BEAS assumes that all coordinates of the boundary are visible from a fixed origin, which is a good approximation for this structure that tends to have a pear-like convex shape. Before refinement of the BEAS contour, the initial circular contour must be defined by parameters, such as the fixed origin and an initial radius. In this work, they are based on properties of the CNN segmentation output. The origin is defined as the center of mass of the CNN output, and the initial radius,  $r_c$ , is the average radius of the CNN segmentation output.

The initial contour can then refine and evolve towards the boundary of the CNN segmentation through the minimisation of a segmentation energy functional. To achieve this, a general localised region-based energy functional for level-set segmentation [14] was used. Barbosa et al. [2] adapted these localisation strategies for BEAS in terms of B-spline coefficients, and the expression of the energy gradient is given as,

$$\nabla_c E = \frac{\partial E}{\partial c[k]} = \int_{\Gamma} g(\theta) \beta^d \left( \frac{\theta - hk}{h} \right) d\theta. \quad (2)$$

The function  $g(\theta)$  represents the features of the object to be segmented and is evaluated over the boundary  $\Gamma$ . In this work, the energy function used was the Localised Yezzi Energy, proposed by Lankton and Tannenbaum et al. [14,28]. This energy depends on the average intensity of the CNN output inside and outside the evolving B-spline contour. The contour evolves to have the maximum separation between them. For Localised Yezzi the feature function is given as,

$$g(\theta) = \frac{(I(\psi(\theta), \theta) - u_\theta)^2}{A_u} - \frac{(I(\psi(\theta), \theta) - v_\theta)^2}{A_v}. \quad (3)$$

$A_u$  and  $A_v$  represent the areas inside and outside of the contour, respectively; and  $u_\theta$  and  $v_\theta$  are the mean intensities inside and outside the evolving contour at the polar angle,  $\theta$ , respectively.  $I(\psi(\theta), \theta)$  corresponds to the image value (i.e. CNN output) at position  $(\rho, \theta)$ . The Yezzi energy relies on the assumption that the interior and the exterior of the contour have the largest difference in average intensities. This is a good assumption for this work, as the goal is to represent the CNN segmentation output as a smooth B-spline contour. The final B-spline coefficients are saved and used in the following section.

**Interaction framework** Finally, the contour formed from the previous step and the corresponding US image are loaded in a window, where the user can interact with the contour. In the interactive framework, the energy function driving BEAS, is compounded of three energy terms: Localised Yezzi of the US image,  $E_U$ , Localised Yezzi of the CNN probability map,  $E_{CNN}$  and an interactive energy function,  $E_i$ . The total energy is given as:

$$E_{total} = \alpha E_U + \beta E_{CNN} + \gamma E_i, \quad (4)$$

where  $\alpha$ ,  $\beta$  and  $\gamma$  are hyper-parameters. Here, the initialised contour is determined by the evolved B-spline coefficients from the previous section, and it will evolve with each user-interaction to minimise the energy function defined.

Finally  $E_i$ , is based on a 2D version of reported work [3], where user-defined coordinates interact with the B-splines. The user can create markers where they want the contour to pass through, these act as anchors attracting the contour. A point introduced by the user can be expressed as  $p_{user} = (\rho_{user}, \theta_{user})$ . The energy function penalises the parametric distance,  $D$ , between the current boundary position and  $p_{user}$  at each B-spline knot. Therefore,  $D$  is defined as

$D = (\rho - \rho_{user})^2$ . The energy term driving the contour towards the user-defined points was proposed in 3D by Barbosa et al. [3], where its minimisation with respect to B-spline coefficients,  $c[\mathbf{k}]$  was demonstrated.  $E_{user}$  is defined as:

$$E_{user} = \int_{\Gamma} \delta(\theta - \theta_{user})(\psi(\theta) - \rho_{user})^2 d\theta, \quad (5)$$

where  $\delta(\theta - \theta_{user})$  corresponds to the Dirac function which is non-zero only at the position  $\theta = \theta_{user}$ . When multiple user-defined points are present, the sum of the parametric distance between the current contour,  $\Gamma$  and the user-defined points is used. This evolves the contour towards multiple user points, detailed information can be found in the paper by Barbosa et al. [3]. As the computational load is small, there is real-time feedback of the effect the modifications make.

## 2.2 Data collection

Analysis of anonymised, archived US images was retrospective, so no ethics committee approval was required by the institute. The CNN was trained on a dataset of 444 2D US images from 213 patients, and corresponding ground truth labels of the levator hiatus. The training dataset comprised of two sets of archived clinical images with expert annotations, acquired by several operators. One dataset used for training, was a private dataset supplied by (GE Healthcare; Zipf, Austria) and the second dataset was a private dataset used in previous studies. 400 images were used for training and 44 were used for validation. The test data included a randomised selection of 30 anonymised 2D US images from 10 symptomatic women assessed at the pelvic floor clinic between March and May, 2019 at \*\*\*\*\*. The US images were obtained from Transperineal US volumes acquired following the clinical protocol defined by Dietz et al. [8] on the Voluson E10 US system (GE Healthcare; Zipf, Austria). The 2D planes that were used to segment and assess the levator hiatus were manually determined by an expert clinician, at rest, during the Valsalva manoeuvre and contraction.

## 2.3 Experimental details

Two clinical experts with over 4 years experience in pelvic floor US, participated in the experiment. They segmented the levator hiatus on 30 2D US images using 4DView Trace (GE Healthcare; Zipf, Austria), 4DView Point (GE Healthcare; Zipf, Austria) and the proposed tool. Prior to the experiment the experts were given a tutorial how to use the new tool. 4DView Trace and Point can be found on the ‘measure - generic area’ function of 4DView (GE Healthcare; Zipf, Austria). In 4DView Trace (GE Healthcare; Zipf, Austria), the contour starts once the user clicks the US image, and it will follow the user’s cursor around the levator hiatus until the user clicks on the US a second time. In 4DView Point (GE Healthcare; Zipf, Austria) the tool will trace the hiatus by the user defining multiple points around the levator hiatus with mouse clicks. The lines that connect the points are straight, therefore, the output segmentation is generalised and not

anatomically accurate (i.e. sharp lines). 4DView Trace and 4DView Point (GE Healthcare; Zipf, Austria) may be referred to as Trace and Point respectively in this paper. Uncertainty-Guided Efficient Interactive Refinement (UGIR) utilises an interaction-based level set for fast refinement of segmentations [26], based on scribbles. The same CNN was used as the proposed model and scribbles were created in 3D Slicer [1,9].

The main aim was to compare the perceived subjective workload of the clinical tools and UGIR against the proposed tool. Therefore, half way through the experiment (after 15 segmentations) and at the end of the experiment, the perceived workload was subjectively evaluated by each expert and for each segmentation technique. To do this the National Aeronautics and Space Administration Task Load Index (NASA-TLX) was used [11]. Finally, the time taken for the expert to segment/edit the levator hiatus contour to a clinically accepted level was measured for each segmentation and compared.

## 2.4 Implementation details

The proposed tool was implemented on a Windows desktop with a 24GB NVIDIA Quadro P6000 (NVIDIA, California, United States). The CNN was implemented using NiftyNet [10], training and inference were ran on the GPU. The network architecture was an adaptation of 2D U-Net [22] with half the number of features [32, 64, 128, 256, 512]. An Adam optimiser, ReLU activation function, weighted decay factor of  $10^{-5}$  and batch size of 64 were used. Whitening and histogram normalisation (i.e. when the image was set to have zero-mean and unit variance) were applied to reduce the effects of noise [18]. A Dice loss function was used, with a learning rate of  $10^{-5}$ . The data augmentation used were: elastic deformation (deformation sigma = 5, number of control points = 4), random scaling (-20%, +20%), vertical ‘flipping’ and an implementation of mixup [29]. Validation of the network training was performed every 250 epochs and the CNN trained for 12,000 epochs. The CNN model from epoch 10,000 was used at inference, as the validation loss function was lowest. The CNN hyper-parameters were determined based on literature [6] and the performance of the training dataset.

BEAS optimisation was ran on the CPU. In task 2, the size of the neighbourhood used to estimate the local intensity of the image was set to 100 pixels (i.e.  $\approx 30mm$ ), allowing the contour to recover from a bad initialisation. For both tasks the BEAS contour was discretised into 32 points (i.e. knots) along the polar angle direction, causing the scale parameter,  $h$ , to be implicitly fixed to 1. The B-spline coefficients,  $c(\mathbf{k})$ , are gathered in a 1D index array, spanning the polar domain with 32 B-spline coefficients. For interactive BEAS, in (4)  $\alpha = 0.5$ ,  $\beta = 0.3$  and  $\gamma = 3$ . The size of the neighbourhood used to estimate the local intensity was set to 10 pixels ( $\approx 3mm$ ). This is low to avoid the contour evolving before user-interaction. Otherwise the contour may evolve towards bright regions of the US in order minimise the energy function. The hyper-parameters used for BEAS were determined by a grid search method where the range was guided by literature [2] and evaluated by assessing the performance of the training dataset.

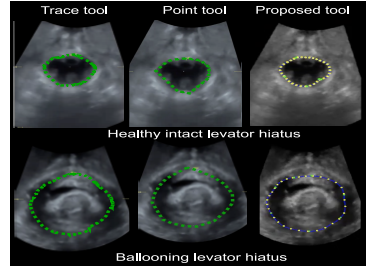


**Fig. 2.** Visual representation of the levator hiatus segmentation obtained with the clinical tools and proposed pipeline, in a healthy patient at contraction and a patient with ballooning hiatus at Valsalva.

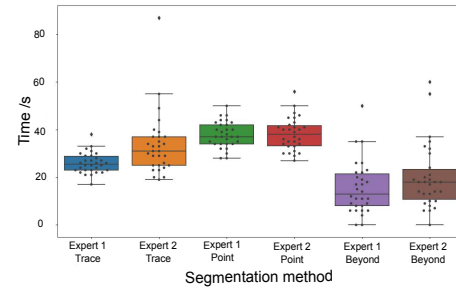


**Fig. 3.** Time taken to delineate the levator hiatus to a clinically acceptable level with 4DView Trace, Point (GE Healthcare; Zipf, Austria) and the proposed tool.

### 3 Results

Fig. 2 shows examples of the segmentation obtained via the clinical tools and the proposed pipeline. The experts agreed that the proposed tool accomplished a clinical acceptable standard for hiatal diagnosis for almost all 2D US images (29 images), thus the proposed tool achieved a ‘clinical acceptability’ of 97%. However, only 2 and 1 CNN + BEAS post-processing segmentation’s required no editing from expert 1 and 2 respectively, equalling a ‘clinical acceptability’ of 5%. The ‘clinical acceptability’ of the CNN alone was 2%, and the ‘clinical acceptability’ of UGIR was 27%.

Fig. 3 shows the time taken for expert 1 and 2 to delineate a segmentation of the levator hiatus to a clinically acceptable standard for diagnosis, using the clinical tools and proposed method. The recorded time of the proposed pipeline does not include CNN inference time, to be solely dependent on user interaction time and independent of the CNN’s performance. The average CNN inference time was  $4.90 \pm 1.58$  seconds. The time taken using the UGIR method was  $63.77 \pm 31.27$  seconds. The time taken to edit the levator hiatus contour with the proposed tool was ‘significantly lower’ (paired t-test,  $p \leq 0.001$ ) than the clinical tools and state of the art method, UGIR. The time taken decreased over the experiment, as the combined mean of the first 15 segmentations was  $19.33 \pm 11.93$  seconds and for the final 15 segmentations was  $16.13 \pm 11.40$  seconds. Table 1 shows the mean NASA-TLX scores of both experts, and table 2 shows the NASA-TLX scores half way through the experiment (attempt 1), and at the end of the experiment (attempt 2). Within the tables the individual weighted sub-scales are reported, as well as the total weighted work-load. The perceived workload was ‘significantly lower’ (paired t-test,  $p=0.001$ ) in the proposed tool than the clinical tools perceived by both experts. It is worth noting a lower score for perceived performance in this table corresponds to a better perceived performance. Therefore, the experts found the proposed tool to perform better than the clinical tools and UGIR. Furthermore, the perceived mental workload

**Table 1.** The perceived weighted workload score from the NASA-TLX questionnaire and individual sub-scale scores that contribute to it are shown. A low weighted workload score corresponds to a tool that requires less effort, less frustration, less mental, temporal and physical demands, and a tool that has a higher perceived performance.

NASA-TLX weighted scores	Average			
	Trace	Point	UGIR	Beyond
Effort	13.67	15.50	14.00	6.17
Frustration	12.00	11.00	21.34	2.17
Mental Demand	14.33	10.84	8.67	6.17
Performance	11.00	18.34	28.34	5.34
Physical Demand	6.67	4.67	4.00	3.67
Temporal Demand	0.84	0.00	0.00	0.34
Total workload	58.47	60.34	76.33	23.84

of the proposed tool improved at the end of the experiment, showing improved performance after exposure to the tool.

## 4 Discussion

Fig. 2 shows visually similar contours for all tools. The proposed method shows more anatomically plausible results than the Point tool. The proposed tool achieved visually ‘clinically acceptable’ results for almost all cases, however, only 2 and 1 CNN segmentations required no editing from expert 1 and 2 respectively. The sub-optimal segmentation was due to a poor US acquisition (that was noted as a clinically unacceptable US image), this reduced the visibility of the levator hiatal boundary, which severely impacted the CNN output. Retrospectively, the radius defining the initial BEAS contour in the second task was increased, and an optimal segmentation was obtained using the proposed tool. Thus, the tool is capable of a ‘clinical acceptability’ score of 100%, with further tuning.

Both experts achieved at least an average improvement of 13 seconds when using the proposed tool. The time measured did not include CNN inference time, to keep it independent to the experiment, and to allow for direct comparison with other segmentation tasks of different CNN architectures. It is assumed with optimisation the CNN inference time would reduce. The proposed tool nonetheless, is still quicker than the clinical tools and UGIR, and it may be assumed with further practice, the time taken would continue to decrease.

Following 30 levator hiatus segmentations, the NASA-TLX questionnaire demonstrated the tool improved perceived performance, reduced effort, frustration, mental and temporal demand. The proposed tool reduced the weighted perceived workload, by 36.50, 34.63 and 52.49 points on the NASA-TLX index scale, for Point, Trace and UGIR tools respectively. The performance improved by 13.00, 5.66, 23.00 points on the NASA-TLX weighted index scale compared to the Point, Trace and UGIR tools respectively. It may be assumed the performance of the Point tool was lower, due to the less anatomically accurate segmentation, shown in Fig. 2. Therefore, it may be assumed that this work could

**Table 2.** The perceived weighted workload score from the NASA-TLX questionnaire and individual sub-scale scores that contribute to it are shown from mid-experiment (attempt 1) and the end of the experiment (attempt 2). A low weighted workload score corresponds to a tool that requires less effort, less frustration, less mental, temporal and physical demands, and a tool that has a higher perceived performance.

NASA-TLX weighted scores	Attempt 1			Attempt 2		
	Trace Point	Beyond	Trace Point	Beyond		
Effort	11.00	14.67	7.33	16.33	16.33	5.00
Frustration	12.00	11.00	3.33	12.00	11.00	1.00
Mental Demand	15.33	9.67	5.33	13.33	12.00	7.00
Performance	10.67	15.00	6.00	11.33	21.67	4.67
Physical Demand	7.00	4.00	3.33	6.33	5.33	4.00
Temporal Demand	1.67	0.00	0.00	0.00	0.00	0.67
Total workload	57.60	54.34	25.34	59.33	66.33	22.33

improve the clinical workflow. Table 2 showed that the perceived workload score was lower at the end of the experiment than at mid-experiment, highlighting that with increased exposure, the workload may continue to reduce.

The proposed tool is compounded of a post-processing filter and an interactive algorithm. It can be easily implemented on other 2D segmentation tasks, to improve the segmentation boundary and allow for easy editing of incorrect segmentation. There is scope to expand this work to 3D segmentation. Currently, the hyper-parameters used for BEAS (i.e. number of B-splines) requires manual optimisation. In future work, it would be beneficial to automate hyper-parameter selection dependent on the initial 2D segmentation, and compare performance for several segmentation tasks.

## 5 Conclusion

To conclude, in this work, a novel CNN-based interactive 2D segmentation tool was proposed. The interactive element works in real-time and requires less user time and perceived workload than current clinical methods, suggesting the proposed work may improve the current clinical workflow. The method utilised the BEAS framework, which ensured the final contour was more biologically plausible than CNN segmentation outputs. This framework can easily be implemented for other 2D segmentation tasks, to make the results more robust while improving the clinical acceptability and giving liability to clinicians.

## 6 Acknowledgments

We gratefully acknowledge General Electric Healthcare (Zif, Austria) , for their continued research support.

## References

1. 3d slicer image computing platform.
2. D. Barbosa, T. Dietenbeck, J. Schaefer, J. D'hooge, D. Friboulet, and O. Bernard. B-spline explicit active surfaces: An efficient framework for real-time 3-d region-based segmentation. *IEEE transactions on image processing : a publication of the IEEE Signal Processing Society*, 21:241–51, 01 2012.
3. D. Barbosa, B. Heyde, M. Cikes, T. Dietenbeck, P. Claus, D. Friboulet, O. Bernard, and J. D'hooge. Real-time 3d interactive segmentation of echocardiographic data through user-based deformation of b-spline explicit active surfaces. *Computerized Medical Imaging and Graphics*, 38:57–67, 01 2014.
4. S. Benjamens, P. Dhunnoo, and B. Mesko. The state of artificial intelligence-based fda-approved medical devices and algorithms: an online database. *npj Digital Medicine*, 3, 09 2020.
5. O. Bernard, D. Friboulet, P. Thevenaz, and M. Unser. Variational b-spline level-set: A linear filtering approach for fast deformable model evolution. *IEEE Transactions on Image Processing*, 18(6):1179–1191, 2009.
6. E. Bonmati, Y. Hu, N. Sindhwan, H. Dietz, J. D'hooge, D. Barratt, J. Deprest, and T. Vercauteren. Automatic segmentation method of pelvic floor levator hiatus in ultrasound using a self-normalising neural network. *Journal of Medical Imaging*, 5, 12 2017.
7. H. P. Dietz, F. Moegni, and K. L. Shek. Diagnosis of levator avulsion injury: a comparison of three methods. *Ultrasound in Obstetrics & Gynecology*, 40(6):693–698, 2012.
8. H. P. Dietz, C. Shek, and B. Clarke. Biometry of the pubovisceral muscle and levator hiatus by three-dimensional pelvic floor ultrasound. *Ultrasound in Obstetrics & Gynecology*, 25(6):580–585, 2005.
9. A. Fedorov, R. Beichel, J. Kalpathy-Cramer, J. Finet, J.-C. Fillion-Robin, S. Pu-jol, C. Bauer, D. Jennings, F. Fennessy, M. Sonka, J. Buatti, S. Aylward, J. V. Miller, S. Pieper, and R. Kikinis. 3d slicer as an image computing platform for the quantitative imaging network. *Magnetic Resonance Imaging*, 30(9):1323–1341, 2012. Quantitative Imaging in Cancer.
10. E. Gibson, W. Li, C. H. Sudre, L. Fidon, D. I. Shakir, G. Wang, Z. Eaton-Rosen, R. Gray, T. Doel, Y. Hu, T. Whyntie, P. Nachev, D. C. Barratt, S. Ourselin, M. J. Cardoso, and T. Vercauteren. Niftynet: a deep-learning platform for medical imaging. *CoRR*, abs/1709.03485, 2017.
11. S. G. Hart. Nasa-task load index (nasa-tlx); 20 years later. *Proceedings of the Human Factors and Ergonomics Society Annual Meeting*, 50(9):904–908, 2006.
12. W.-D. Jang and C.-S. Kim. Interactive image segmentation via backpropagating refinement scheme. In *Proceedings of The IEEE Conference on Computer Vision and Pattern Recognition*, 2019.
13. S. N. Kumar, A. L. Fred, and P. S. Varghese. An overview of segmentation algorithms for the analysis of anomalies on medical images. *Journal of Intelligent Systems*, 29(1):612–625, 2020.
14. S. Lankton and A. Tannenbaum. Localizing region-based active contours. *IEEE Transactions on Image Processing*, 17, 12 2008.
15. X. Li, Y. Hong, D. Kong, and X. Zhang. Automatic segmentation of levator hiatus from ultrasound images using u-net with dense connections. *Physics in Medicine and Biology*, 64, 03 2019.

16. D. Lin, J. Dai, J. Jia, K. He, and J. Sun. Scribblesup: Scribble-supervised convolutional networks for semantic segmentation. *CoRR*, abs/1604.05144, 2016.
17. K. Maninis, S. Caelles, J. Pont-Tuset, and L. V. Gool. Deep extreme cut: From extreme points to object segmentation. *CoRR*, abs/1711.09081, 2017.
18. K. K. Pal and K. S. Sudeep. Preprocessing for image classification by convolutional neural networks. In *2016 IEEE International Conference on Recent Trends in Electronics, Information Communication Technology (RTEICT)*, pages 1778–1781, 2016.
19. D. L. Pham, C. Xu, and J. L. Prince. Current methods in medical image segmentation. *Annual Review of Biomedical Engineering*, 2(1):315–337, 2000. PMID: 11701515.
20. M. Rajchl, M. C. H. Lee, O. Oktay, K. Kamnitsas, J. Passerat-Palmbach, W. Bai, B. Kainz, and D. Rueckert. Deepcut: Object segmentation from bounding box annotations using convolutional neural networks. *CoRR*, abs/1605.07866, 2016.
21. H. Ramadan, C. Lachqar, and H. Tairi. A survey of recent interactive image segmentation methods. *Computational Visual Media*, 08 2020.
22. O. Ronneberger, P. Fischer, and T. Brox. U-net: Convolutional networks for biomedical image segmentation. *CoRR*, abs/1505.04597, 2015.
23. T. Sakinis, F. Milletari, H. Roth, P. Korfiatis, P. M. Kostandy, K. Philbrick, Z. Akkus, Z. Xu, D. Xu, and B. J. Erickson. Interactive segmentation of medical images through fully convolutional neural networks. *CoRR*, abs/1903.08205, 2019.
24. S. A. Taghanaki, K. Abhishek, J. P. Cohen, J. Cohen-Adad, and G. Hamarneh. Deep semantic segmentation of natural and medical images: A review. *CoRR*, abs/1910.07655, 2019.
25. M. Unser. Splines: A perfect fit for signal and image processing. *IEEE Signal Processing Magazine*, pages 22 – 38, Nov. 1999.
26. G. Wang, M. Aertsen, J. Deprest, S. Ourselin, T. Vercauteren, and S. Zhang. *Uncertainty-Guided Efficient Interactive Refinement of Fetal Brain Segmentation from Stacks of MRI Slices*, pages 279–288. 09 2020.
27. G. Wang, W. Li, M. A. Zuluaga, R. Pratt, P. A. Patel, M. Aertsen, T. Doel, A. L. David, J. Deprest, S. Ourselin, and T. Vercauteren. Interactive medical image segmentation using deep learning with image-specific fine-tuning. *CoRR*, abs/1710.04043, 2017.
28. A. Yezzi, A. Tsai, and A. Willsky. A fully global approach to image segmentation via coupled curve evolution equations. *J. Vis. Commun. Image Represent.*, 13:195–216, 2002.
29. H. Zhang, M. Cissé, Y. N. Dauphin, and D. Lopez-Paz. mixup: Beyond empirical risk minimization. *CoRR*, abs/1710.09412, 2017.